# CUME EXAM # 398 - WITH SUGGESTED SOLUTIONS

This exam is worth 61 points. It is based on the accompanying paper by Berné et al. (2015), "Very Large Telescope observations of Gomez's Hamburger: Insights into a young protoplanetary candidate," arXiv:1504.02735 [astro-ph.GA]. A grade of 70% or higher is expected to be a passing grade. You may use a calculator, but only for algebraic and trigonometric types of calculations — you may NOT use a calculator to store formulae, constants, etc.

# Things You Might Need to Know

 $\begin{array}{l} 1 \; \mathrm{AU} = 1.496 \, \times \, 10^{11} \; \mathrm{m} \\ 1 \; \mathrm{pc} = 3.086 \, \times \, 10^{16} \; \mathrm{m} \\ G = 6.674 \, \times \, 10^{-11} \; \mathrm{N} \; \mathrm{m}^2 \; \mathrm{kg}^{-2} \\ \mathrm{L}_{\odot} = 3.8 \, \times \, 10^{26} \; \mathrm{W} \\ \mathrm{M}_{\odot} = 1.9891 \, \times \, 10^{30} \; \mathrm{kg} \\ \mathrm{R}_{\odot} = 6.955 \, \times \, 10^8 \; \mathrm{m} \\ \sigma = 5.670 \, \times \, 10^{-8} \; \mathrm{W} \; \mathrm{m}^{-2} \; \mathrm{K}^{-4} \\ \mathrm{m}_p = 1.6726 \, \times \, 10^{-27} \; \mathrm{kg} \\ \mathrm{k} = 1.3806 \, \times \, 10^{-23} \; \mathrm{m}^2 \; \mathrm{kg} \; \mathrm{s}^{-2} \; \mathrm{K}^{-1} \\ 1 \; \mathrm{erg} = 10^{-7} \; \mathrm{J} \end{array}$ 

# **Additional Instructions**

- Start each question on a new page and then staple your packet of pages together at the end. Put your name on every page.
- Write legibly! If I cannot read your writing, you likely will not receive as much credit
  as you deserve because I won't understand what you're trying to convey.

# GoHam Properties

1. Shortly after its discovery in 1987, Gomez's Hamburger (a.k.a. GoHam) was thought to be a post-AGB nebula (a pre-planetary nebula). Now it is recognized as an edge-on protoplanetary disk. What kind(s) of "recent studies" (cited in the second paragraph of the Introduction) do you think could have led to this newer interpretation? (5 points)

High-resolution CO mapping of GoHam revealed that the nebula is essentially a disk in keplerian rotation. As it turns out, the rotation velocity yields a relatively high mass for the central star(s). The derived central stellar mass and luminosity are not compatible with those acceptable for post-AGB sources, but are very similar to those expected in pre-MS A stars.

2. The distance to GoHam was originally determined from its integrated flux distribution, derived from photometric observations of the object (shown below in Fig. 1). Integrating the GoHam flux in Fig. 1 yields an apparent

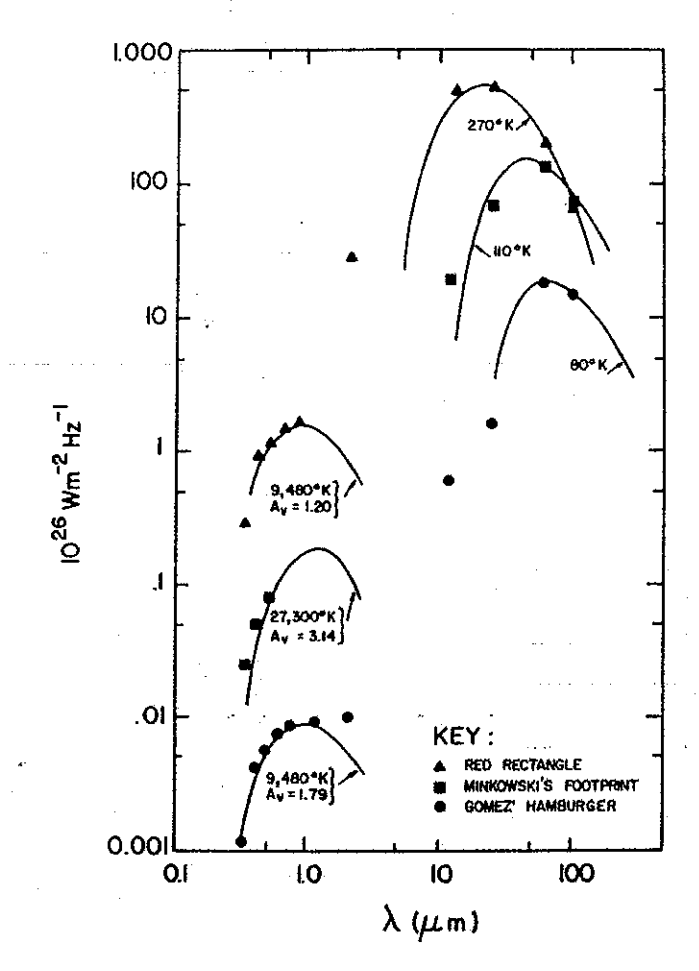


FIG. 4.—Flux distribution for "Gomez's Hamburger" shown along with those for the Red Rectangle and Minkowski's Footprint. Blackbodies have been fitted to their optical and infrared fluxes.

Figure 1: From Ruiz et al. (1987), ApJL 316, L21.

bolometric luminosity of  $1.1 \times 10^{-9}$  ergs cm<sup>-2</sup> s<sup>-1</sup>.

a) Use this information to compute the distance to GoHam; give your final answer in units of pc. State whatever assumptions you make about the central star. (7 points)

A rough estimate of the distance can be obtained by using  $L = 4\pi R^2 \sigma T^4$  and  $F = L/(4\pi r^2)$ . So  $1.1 \times 10^{-9}$  ergs cm<sup>-2</sup> s<sup>-1</sup> =  $(R/d^2)\sigma T^4$ . You have to make some assumptions about the radius and temperature of the pre-MS A star. If you assume T  $\sim 10{,}000$  K and  $R \sim 10 \times R_{\odot}$ , you get a distance value of  $\sim 2$  kpc. This is what Ruiz

originally did, and it turned out to be too large by about an order of magnitude!

b) Compare your distance result to the value given in the paper for this exam. If the two values are different, discuss any possible sources of the discrepancy. (4 points)

Sources of any discrepancy would likely be extinction due to dust, which you likely didn't account for in the above calculation, and not knowing the exact value for T (or F) for the star.

# Observations

The new data presented in this paper were acquired with the Very Large Telescope at Cerro Paranal in Chile. The VLT consists of four 8.2-m "unit telescopes" (UTs), which can be operated independently or interferometrically (as VLTI). The positions of the UTs are fixed and their baselines range from 46.6 to 130.2 m in length. The interferometer also includes four 1.8-m "auxiliary telescopes" (ATs), which can be moved to different positions. Their baseline distances range between 11.3 and 153.0 m.

3. Compare the angular resolution of one of the UTs (at one of the wavelengths used for this study) to the best angular resolution achievable with the ATs working as an interferometer at the same wavelength. You may assume that the UT is equipped with adaptive optics, resulting in near-diffraction-limited observations. (6 points)

For the UT, angular resolution  $\theta \sim 1.22 \ \lambda/D$ . If  $\lambda = 8.6 \ \mu m$  (corresponding to the PAH1 filter) and  $D = 8.2 \ m$ ,  $\theta = 1.280 \times 10^{-6} \ rad = 0.264$  arcsec. For the AT, if we take D as the maximum baseline distance of 153.0 m, then  $\theta = 6.858 \times 10^{-8} \ rad = 14.1 \ milliarcsec$ .

4. Briefly discuss how an interferometer works. In your discussion, you should include the general physical principles, what actually gets observed and how the data get turned into a map, and the challenges that are inherent with doing interferometry. (10 points)

Points to include are:

- involves multiple telescopes that are separated by known spacing
- allows them to act as a large telescope w/effective area dictated by largest baseline

- light wavefronts that reach the telescopes are at different-phases
- the phase and intensity signals (interference patterns) from each telescope are combined using a correlator
- using Fourier transforms can produce radio maps of target
- challenges include accounting for noise sources and knowing the precise separation between the elements of an interferometer (becomes more challenging at shorter wavelengths!)
- 5. The observations discussed in this paper were acquired with one of the UTs acting as a stand-alone telescope. The paper mentions a *chopping-nodding* mode when describing the data acquisition. What does this mean, and why would this mode be used? (3 points)

Chopping-nodding corresponds to a rapid switching motion of the secondary mirror so that one can obtain frequent images of the sky. The sky background is a) large and b) highly variable in the IR, and chopping or nodding the telescope allows one to obtain sky frames that are nearly coincident with the science frames, which enables a more accurate removal of the sky background.

6. The VLT observations were compared with Sub-Millimeter Array (SMA) maps of the <sup>12</sup>CO(2-1) and <sup>13</sup>CO(2-1) lines. What kind of transitions are these? (in other words, what is physically happening to give rise to this emission?) (5 points)

These are rotational transitions of the CO molecule. Molecules rotate along their different axes, but the rotational energies are quantized. A rotational transition takes place when the molecule transitions from one rotational energy level to another by gaining or losing a photon. The rotational energy is going from the  $2^{nd}$  level to the  $1^{st}$  level in this case (given by the rotational quantum number, J). Rotational lines are typically seen in the radio/mm region of the electromagnetic spectrum.

7. Why would the team be looking at both <sup>12</sup>CO and <sup>13</sup>CO lines? What information could be gained by doing so? And are there other lines that you think could provide additional useful information? (5 points)

<sup>12</sup>CO lines can be optically thick, but since <sup>13</sup>CO is much less abundant, it is less likely to be optically thick and therefore can be used to derive molecular gas densities. Other isotopologues of CO could also be used for the same purpose (e.g. C<sup>18</sup>O). Other molecules could also be used to probe localized regions of high gas density (e.g. CS,

# Planet Formation and Disk Physics

Here we will explore the Toomre Q parameter as a means of determining whether the GoHam disk is unstable to collapse through gravitational instability.

8. When considering whether a protoplanetary disk may gravitationally fragment to form planets, we balance three timescales to get the Toomre Q parameter: the free-fall time scale, the acoustic crossing time (which can also be thought of as pressure), and the Keplerian shear time scale. In this fashion,

$$Q \equiv \frac{c_s \Omega}{\pi G \Sigma} \tag{1}$$

Explain how the above three timescales are manifested within the expression for Q. You don't have to completely derive the equation for Q, but explain where each of the variables in Eq. (1) above comes from. [ $\Sigma$  is the surface density.] (8 points)

If you consider a clump of scale  $\Delta r$  and mass  $\Delta m \sim \pi (\Delta r)^2 \Sigma$ , if it were in isolation the clump would collapse on the free-fall timescale

$$t_{ff} \sim \sqrt{\frac{\Delta r^3}{GM}} \sim \sqrt{\frac{\Delta r}{\pi G \Sigma}}$$
 (2)

This collapse would be balanced by pressure and rotational shear. The acoustic crossing time ( $\sim$  pressure) is given by  $t_p \sim \frac{\Delta r}{c_s}$  where  $c_s$  is the sound speed in the disk. The Keplerian shear time scale is given by

$$t_{shear} \sim \frac{1}{r} \left(\frac{d\Omega}{dr}\right)^{-1} \sim \Omega^{-1}$$
 (3)

Given the above, the terms in the Toomre disk stability criterion, Q, can now be seen to come from each of the above timescales:  $\pi G\Sigma$  coming from  $t_{ff}$ ,  $c_s$  coming from  $t_p$ , and  $\Omega$  coming from  $t_{shear}$ .

9. What are the physical processes that result in radial flaring (increasing disk scale height vs. radial distance from the central star) and what does that structure imply about the ratio of disk-to-star mass? (8 points)

The gravity term in the equation of hydrostatic equilibrium is what dominates here. The vertical scale height of the disk is inversely proportional to g, so as g decreases at large radial distances, H increases and the disk flares out. This implies that the star's mass is much larger (factors of 10's to 100's) than the disk mass.

# **Very Large Telescope observations of** *Gomez's Hamburger:* **Insights into a young protoplanet candidate** \*

O. Berné<sup>1, 2</sup>, A. Fuente<sup>3</sup>, E. Pantin<sup>4</sup>, V. Bujarrabal<sup>3</sup>, C. Baruteau<sup>1, 2</sup>, P. Pilleri<sup>1, 2</sup>, E. Habart<sup>5</sup>, F. Ménard<sup>6, 7, 8</sup>, J. Cernicharo<sup>9, 10</sup>, A. G. G. M. Tielens<sup>11</sup>, and C. Joblin<sup>1, 2</sup>

<sup>1</sup> Université de Toulouse; UPS-OMP; IRAP; Toulouse, France

<sup>2</sup> CNRS; IRAP; 9 Av. colonel Roche, BP 44346, F-31028 Toulouse cedex 4, France

Observatorio Astronómico Nacional, Apdo. 112, 28803 Alcalá de Henares, Madrid, Spain.

Service d'Astrophysique CEA Saclay, France

- Institut d'Astrophysique Spatiale, Paris-Sud 11, 91405 Orsay, France
- Millenium Nucleus "Protoplanetary Disks in ALMA Early Science," Universidad de Chile, Casilla 36-D, Santiago, Chile
- <sup>7</sup> UMI-FCA 3386, CNRS/INSU, Casilla 36-D, Santiago, Chile
- <sup>8</sup> Univ. Grenoble Alpes, IPAG, F-38000 Grenoble, France

CNRS, IPAG, F-38000 Grenoble, France

- <sup>9</sup> Instituto de Ciencia de Materiales de Madrid (ICMM-CSIC). Sor Juana Ines de la Cruz 3, 28049 Cantoblanco, Madrid, Spain.
- Centro de Astrobiología, CSIC-INTA, Ctra. de Torrejón a Ajalvir km 4, E-28850 Madrid, Spain.
- Leiden Observatory, Leiden University, Niels Bohrweg 2, NL-2333 CA Leiden, The Netherlands.

#### **ABSTRACT**

Planets are thought to form in the gas and dust disks around young stars. In particular, it has been proposed that giant planets can form via gravitational instability of massive extended disks around intermediate mass stars. However, direct observations to constrain this mechanism lack. We have spatially resolved the 8.6 and 11.2  $\mu$ m emission of a massive edge on protoplanetary disk around an A star, Gomez's Hamburger (GoHam), using VISIR at the Very Large Telescope. A compact region situated at a projected distance of 350  $\pm$  50 AU South of the central star is found to have a reduced emission. This asymmetry is fully consistent with the presence of a cold density structure, or clump, identified in earlier CO observations, and we derive physical characteristics consistent with those observations: a mass of 0.8-11.4 Jupiter masses (for a dust to gas mass ratio of 0.01), a radius of the order of  $10^2$  astronomical units, a local density of the order of  $10^7$  cm<sup>-3</sup>. Based on this evidence, we argue that this clump, which we call GoHam b, is a promising candidate for a young protoplanet formed by gravitational instability, that could be representative of the precursors of massive planets observed around A stars, like HR 8799 or Beta-pictoris. Further studies at high angular resolution are needed to better constrain the physical properties of this object in order to confirm this proposal.

# 1. Introduction

The disks present around low to intermediate mass young stellar objects have gained much interest in the recent years since they are believed to be the cradles of planetary formation. In this context, the study of their dust and gas content is crucial, because dust is the primary reservoir of matter to form telluric planets and the cores of giant planets. The recent discoveries by direct imaging techniques of over 20 giant planets with orbital separations from 10 to few hundred AU suggest that giant planets can form in the outer regions of protoplanetary disks. In these regions disks can become unstable to their own gravity and form clumps of molecular gas which can continue to accrete mass and later evolve towards planets (or brown dwarfs). This "gravitational instability" (GI, e.g., Boss 1997) scenario is a likely channel for planet formation around A or B stars. Direct observations of giant planets around the A stars HR 8799 and Beta-pitoris with estimated separations between several 10 AUs (Marois et al. 2010; Lagrange et al. 2010), support this idea, however, direct evidence of GIs, or protoplanets resulting from GIs, are rare. One possible example of a candidate protoplanet was provided recently by Quanz et al. (2013, 2014), who identified a source in the disk around the Herbig star HD 100456, at a projected separation of  $\sim 50$  AU. The mass of this source could not be derived directly, but is at most a few Jupiter mass (Boccaletti et al. 2013; Currie et al. 2014).

Gomez's Hamburger (IRAS 18059-3211; hereafter GoHam) is an A star surrounded by a dusty disk. When first studied by Ruiz et al. (1987), it was classified as an evolved object (post-AGB star) on the basis of its spectral type and the presence of dust. However, all recent studies (Bujarrabal et al. 2008; Wood et al. 2008; Bujarrabal et al. 2009; De Beck et al. 2010) clearly indicate that it is a young A star surrounded by a protoplanetary disk. The distance to GoHam is not known precisely. but a value  $d = 250 \pm 50$  pc is required to satisfy all the existing observational constraints (Wood et al. 2008; Berné et al. 2009; Bujarrabal et al. 2009). We will adopt this value with the uncertainty throughout the paper. GoHam presents intense CO emission, SMA maps of <sup>12</sup>CO and <sup>13</sup>CO J=2-1 lines very clearly show the Keplerian dynamics of the disk (Bujarrabal et al. 2008, 2009). The lower limit for the disk mass derived from these CO observations is of the order of 10<sup>-2</sup> M<sub>☉</sub>, while the mass upper limit is estimated to be ~ 0.3 M<sub>o</sub> based on dust emission (Bujarrabal et al. 2008; Wood et al. 2008) and assuming an interstellar dust to gas mass ratio of 0.01. Overall, GoHam appears to be similar to isolated Herbig stars (Meeus et al. 2001) such as HD 100546 and HD 169142, in a more massive version but still smaller than the recently discovered disk around CAHA

<sup>\*</sup> Based on observations collected at the European Southern Observatory, Chile under program ID 385.C-0762A.

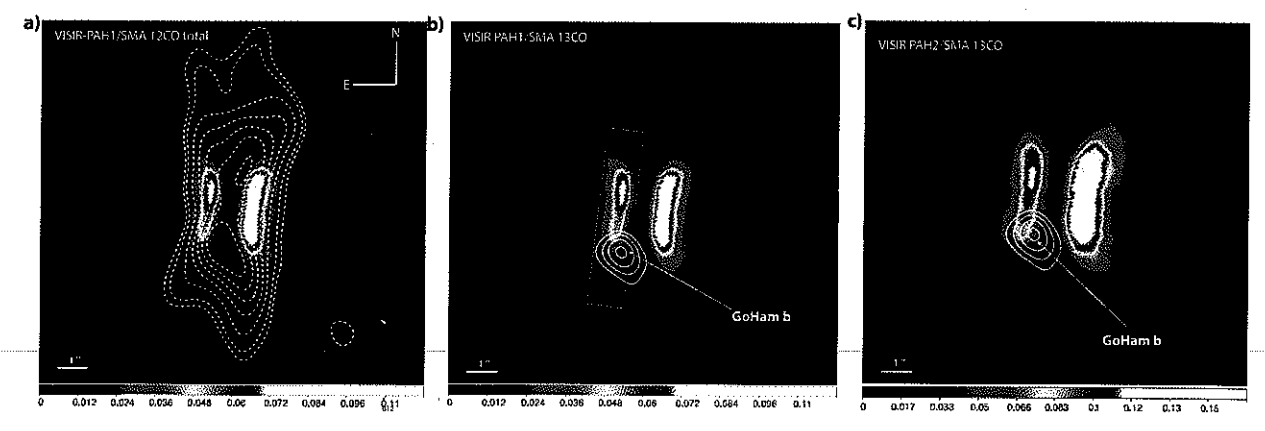


Fig. 1. a) VLT-VISIR 8.6  $\mu$ m (PAH1 filter) image of GoHam in color, the scale is in Jy/arcsec<sup>2</sup>. In contours: velocity integrated  $^{12}$ CO(2-1) emission observed with the SMA from Bujarrabal et al. (2008, 2009). b) VLT-VISIR 8.6  $\mu$ m (PAH1 filter, same as left panel) in color. Contours show the emission of  $^{13}$ CO (2-1) emanating from from GoHam b after subtraction of the best fit disk model (see Bujarrabal et al. 2009 for details). This region also corresponds to the local decrease of mid-IR emission seen in the VISIR image. The position of the cross cut used to extract the profiles shown in Fig. 3 is shown in green. c) VLT-VISIR 11.2  $\mu$ m (PAH2 filter) image of GoHam in color, the scale is in Jy/arcsec<sup>2</sup>. Contours as in b).

J23056+6016 (Quanz et al. 2010). GoHam is seen almost perfectly edge-on, which offers the possibility to study this class of objects from a new and complementary perspective, and in particular with improved constraints on the vertical structure of the disk. Using a radiative transfer model to predict line emission from a Keplerian flaring disk, Bujarrabal et al. (2009) derived a large-scale description of the physical conditions throughout the disk. After subtraction of the best fit model to the observations, these authors found a significant residual emission situated about 1.3" (330  $\pm$  70 AU) South of the central star, which they identified as a gas condensation, containing a mass between 1 and few times that of Jupiter. Hence, this source was proposed to be a candidate protoplanet possibly resulting from a GI collpapse.

GoHam shows bright polycyclic aromatic (PAH) emission (Wood et al. 2008; Berné et al. 2009), as often observed towards Herbie Ae/Be stars (Acke & van den Ancker 2004; Habart et al. 2004). In this letter, we present high angular resolution imaging of GoHam obtained in the PAH filters with VISIR at the Very Large Telescope, which provide a new view of the vertical structure of the disk.

# 2. Observational results

#### 2.1. Observations

GoHam was observed with VISIR at the Very Large Telescope. We obtained three exposures in chopping-nodding in the PAH1 filter (8.6  $\mu$ m) on April 22-23 2010, and two exposures in the PAH2 filter (11.3  $\mu$ m) on August 29 2010 and September 01 2010. The total integration time was 1552 seconds for the PAH1 filter and 1702 seconds for the PAH2 filter. Observations in the PAH1 filter were conducted with an exceptional seeing of 0.5" while the observations in the PAH2 filter were conducted with a seeing ranging between 1.0 and 1.6". Calibration was achieved using the ESO provided observation of the standard star HD 177716. In addition, we use the sub-millimeter array (SMA) data for the  $^{12}$ CO(2-1) and  $^{13}$ CO(2-1) lines observed in June 2006 and presented in Bujarrabal et al. (2009) with a beam size of  $\sim 1.1 \times 1.5$ ". The VISIR and part of the SMA observations are shown in Fig. 1.

#### 2.2. Disk morphology as seen with PAHs

The images obtained in the PAH1 and PAH2 filters are shown in Fig. 1. The observed mid-IR emission results from UV excited polycylic aromatic hydrocarbons (PAHs, Tielens 2008). The PAH1 filter covers part of the C-C vibration at 7.7  $\mu$ m and the C-H vibration at  $8.6 \mu m$ , while the PAH2 filter covers mainly the C-H vibration at 11.3  $\mu$ m (see Fig. A.1). The edge-on disk is clearly resolved, and both faces are separated by a dark lane. where the disk becomes optically thick to its own mid-IR light. This lane is 1.5" broad, i.e.  $375 \pm 75$  AU, larger than what can be observed for any other disk in the mid-IR and suggestive of the massive nature of GoHam. In both images, there is an asymmetry in the fluxes found on the West and East faces of the disk, due to the slight inclination of the disk on the line of sight ( $\sim 5 - 10^{\circ}$ ). The radial extent of the PAH emission ( $R_{PAH} \sim 3^{\circ}$ ) i.e. 750 ± 150 AU) is much smaller than the radial extent observed for the molecular gas in CO (2-1) emission ( $R_{mol} \sim 6.6$ " i.e.  $1650 \pm 350$  AU). On the other hand, the PAH emission extends to higher altitudes ( $H_{PAH} \sim 770 \pm 150 \text{ AU}$ ) above the disk than CO emission ( $H_{mol} \sim 450 \pm 90$  AU, see Bujarrabal et al. 2009). In photodissociation regions, PAH molecules emit mainly in the warm atomic gas as evidenced for instance by the strong spatial correlation with the [CII] fine structure line (Joblin et al. 2010). Therefore, and since they are dynamically coupled to the gas, PAHs can be considered as a tracer of the warm (few 100 K, Joblin et al. 2010) external layers of protoplanetary disks. This warm gas is therefore expected to have a higher scale height than the cold molecular gas traced by low-J CO emission. The proposed morphology is shown in Fig. 2.

# 2.3. Recovery of the GoHam b condensation in absorption in the mid-IR

Since the PAH emission arises from the surface layers of the flared disk, this PAH emission has to go through the disk before reaching us (Fig. 2). At high altitudes the crossed disk slice is thin, and PAH emission is marginally absorbed by the disk. On the other hand, at lower altitudes the PAH emission has to go through part of the disk and is largely absorbed. Absorption at mid-infrared wavelengths is caused by the strong absorption at mid-infrared wavelengths is caused by the strong absorp-

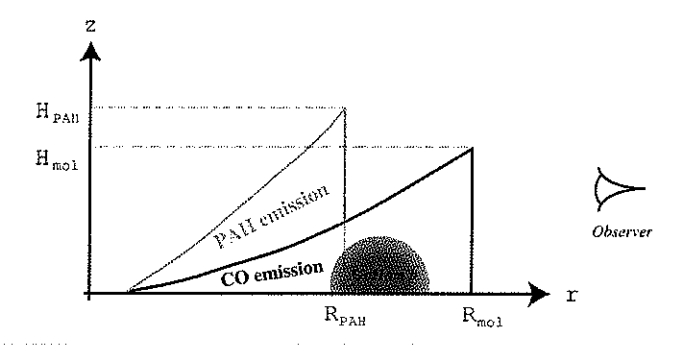


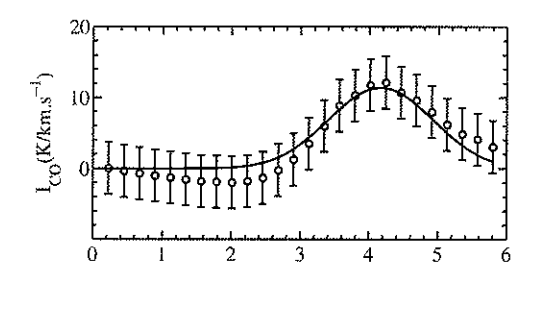
Fig. 2. Schematic representation of the different components of Go-Ham's disk with the main geometrical parameters.

tion band at 9.7  $\mu$ m due to silicates present in dust grains. The beam averaged mid-infrared spectrum of GoHam obtained with Spitzer is shown in Fig. A.1. We fit this spectrum using the PAH-TAT toolbox¹ which allows to adjust an observed spectrum using a set of PAH template spectra, an underlying continuum and a correction for extinction due to silicates (see Pilleri et al. 2012 for details). The results of this procedure are shown in Fig. A.1 and demonstrate that the average spectrum of GoHam is indeed affected by absorption of silicates, with optical depth of the order of 0.4-0.5 at the wavelengths of the VISIR filters.

After subtraction of their radiative transfer model, Bujarrabal et al. (2009) found a residual gas emission in the disk, identified as a condensation of molecular gas. Panels b) and c) of Fig 1 show this residual <sup>13</sup>CO emission tracing the gas condensation, overlaid on the PAH1 and PAH2 images. It can be clearly seen that the condensation spatially corresponds to a local decrease of PAH emission, where the disk is typically less bright by 30%, as compared to the symmetric region in the North. This asymmetry is clearly visible in the profile (Fig. 3) obtained along the cross cut shown in Fig. 1, and indeed seems to match the position of the CO clump. Overall, we conclude that we have likely detected the condensation reported by Bujarrabal et al. (2009) as absorption in the PAH1 and PAH2 filters of VISIR2. From an observer's point of view, this condensation is therefore similar to infrared dark clouds seen against bright mid-IR backgrounds, which are believed to be pre-stellar cores embedded in molecular clouds (Rathborne et al. 2006). GoHam b can be seen as such a core, but embedded in a molecular disk. In the following, we refer to this condensation as GoHam b, following the nomenclature adopted by Quanz et al. (2013).

# 3. Physical properties of GoHam b

In the VISIR images (Fig. 1), GoHam b corresponds to a region of increased absorption. This can be understood as resulting from a localized increase of dust and gas column density at the position where Bujarrabal et al. (2009) detected an excess of CO emission. In order to gain more insights into the properties of GoHam b, we have modeled the mid-IR and <sup>13</sup>CO emission profiles shown in Fig. 3 with a simple parametric model (see



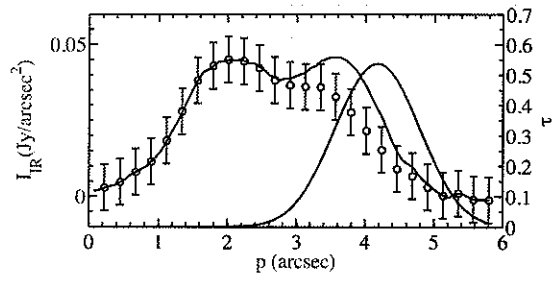


Fig. 3. Emission profiles obtained along the cut shown in Fig. 1. The upper panel presents the observed  $^{13}$ CO (2-1) emission of GoHam b (circles with error bars) and the fit obtained with the model ( $I_{CO}$  see Appendix B) in red. The lower panel shows the observed mid-IR emission profile ( $I_{IR}$ ) for the same cut (circles with error bars), and the mid-IR profile obtained after correction for extinction due to GoHam b ( $I_{IR}^0$ ) in black. The red curve shows the optical depth profile  $\tau_b$  used for this correction.

Appendix B). The model is adjusted so as to reproduce the  $^{13}$ CO profile and to obtain a mid-IR profile corrected from absorption that is symmetric (see Fig. 3). With this model, we derive a radius of GoHam b of  $155 \pm 31$  AU, a density  $n_b = 7.0 \pm 1.4 \times 10^6$  cm<sup>-3</sup> and a mass  $M_b = 0.95 \pm 0.19$  M<sub>Jup</sub>. If the dust cross section per H atom is divided by a factor of 10 as can be the case for protoplanetary disks (Andrews et al. 2009; D'Alessio et al. 2001), then the density and mass are higher by one order of magnitude (i.e.  $M_b = 9.5 \pm 1.9$  M<sub>Jup</sub> and  $n_b = 7.0 \pm 1.4 \times 10^7$  cm<sup>-3</sup>). The final mass range is therefore  $M_b = 0.8 - 11.4$  M<sub>Jup</sub>, a value that is in good agreement with earlier estimates by Bujarrabal et al. (2009) who found masses ranging between 1 and a few Jupiter masses.

#### 4. GoHam b : a candidate protoplanet ?

#### 4.1. Comparison to other substructures seen in disk

In the recent years, high angular resolution observations have revealed the presence of asymmetric features inside protoplanetary disks. In this context, it is interesting to compare the condensation seen in GoHam to other structures observed in disks. Spiral arms have been observed in several disks (e.g. Muto et al. 2012; Casassus et al. 2012; Rameau et al. 2012; Tang et al. 2012; Grady et al. 2013; Boccaletti et al. 2013; Avenhaus et al. 2014), however it seems difficult to understand GoHam b as a spiral arm since it is a unique, unresolved, dense and isolated source in the disk, while spiral arms are generally extended and/or multiple and not necessarily emanating from dense regions. GoHam b could be an arc or horseshoe structure as have been observed in the disks around Oph-IRS 48 (van der Marel et al. 2013; Bruderer et al. 2014), and HD 142157 (Casassus et al.

http://userpages.irap.omp.eu/ cjoblin/PAHTAT/Site/PAHTAT.html

<sup>&</sup>lt;sup>2</sup> Note that, although the SMA and VISIR observations are separated by several years, the source has not moved. This is consistent with the orbital period which is larger than 200 years for a clump on a orbit which is at least 350 AU.

2013). However, this type of asymmetries concerns the emission of dust only, whereas here, both dust (as traced by the  $8.6~\mu m$  optical depth or the millimeter emission, see Fig. 1 in Bujarrabal et al. 2008) and gas column densities are higher towards GoHam b. While we cannot rule out an hypothetical arcstructures made of both gas and dust, there is to our knowledge no observational evidence for such phenomenon so far.

An asymmetry in the mid-IR PAH emission of the edgeon disk around the Herbig Star PDS 144N was reported by Perrin et al. (2006), and appears very similar to the one observed here. Unfortunately there are no spatially resolved observations of the molecular emission of this disk that would attest to the similarity of this structure with GoHam b.

Near-IR observations of scattered light from edge-on disks are generally characterized by asymmetric disk structures, often attributed to illumination effects. The most striking example of such an asymmetry is observed in the HH 30 disk (Stapelfeldt et al. 1999). At IR wavelengths it is the fluorescence of UV excited PAHs which dominates the emission, hence UV illumination effects could also create the observed asymmetry. While we cannot exclude this possibility, the scenario of illumination effects cannot explain the coincidence of the mid-IR emission decrease with the position of the molecular emission. We also note that illumination effects are usually variable in time in such systems, and the Hubble space telescope images of GoHam obtained in the visible and near IR do not show evidence of such variability (see images in Bujarrabal et al. 2008 and Wood et al. 2008).

# 4.2. Comparison to candidate protoplanets

Recently, Quanz et al. (2013) identified a point source in the disk around HD 100546, a Herbig star of B9 spectral type. These authors suggested that this source could represent early stages of planetary formation, and coined the object HD 100546 b. This source shares similarities with GoHam b since it appears as an isolated "clump" inside a massive disk around an intermediate mass star. The mass of HD 100546 b is not well constrained but is estimated to range between 1 and 15  $M_{Jup}$  (Quanz et al. 2013; Boccaletti et al. 2013; Currie et al. 2014), i.e. comparable to GoHam b. However, GoHam b is situated at a much larger distance (330  $\pm$  70 AU) from its host star than HD 100546 b (~ 50 AU). In addition, Quanz et al. (2014) derived an effective temperature of ~ 1000 K for HD 100546 b, while GoHam b appears to be a rather cold object (at most few tens of K according to the CO emission). While the orbit of GoHam b may seem large, it is not exceptional in the context of the recent discovery of a 5  $M_{Jup}$  planet separated from its host star HD 106906 by 650 AU (Bailey et al. 2014). Finally, it should be noted that Dutrey et al. (2014) also reported a clump of molecular gas at the outer edge of the disk ring around GG Tau A, at a radius of ~ 250 AU. Although this latter clump is poorly studied it appears quite similar to GoHam b.

## 4.3. A young protoplanet resulting from a GI?

Since both HD 100546 b and GoHam b are found at large radii and inside massive disks, a natural interpretation for their origin is the gravitational instability as suggested by Quanz et al. (2013). Hydrodynamical models indicate that GI clumps have a typical size of the order of  $\sim 0.4 \times H$  (Boley et al. 2010), where H is the disk scale height inferred from the midplane temperature and the angular velocity. With a minimal orbit of

 $350 \pm 50$  AU for the clump, and using the disk parameters in Table B.1 yields a minimum radius of  $r = 0.4H = 30 \pm 5$  AU, of the same order of magnitude as the value derived from the model:  $r_b = 135 \pm 15$  AU (see Appendix B). Using Eq. (12) of Boley et al. (2010) we derive a theoretical mass for a GI clump at  $350 \pm 50$  AU of  $5.5\pm 1$  M<sub>Jup</sub>, which falls in the mass range derived in Sect. 3 of 0.8 - 11.4 M<sub>Jup</sub>. We can estimate the midplane density  $n_I$  required for the disk to be unstable to the GI at the radius corresponding to the angular separation at which GoHam b is observed, using the classical Toomre Q parameter (Toomre 1964). For the physical conditions in Table B.1, we find that the disk is unstable, i.e. that  $Q \le 2$  for a density larger than  $n_I \sim 2 \times 10^8 \text{cm}^{-3}$ , in agreement with the observed lower limit  $n > 10^6 \text{cm}^{-3}$  derived from CO observations (Table B.1).

#### 5. Conclusion

Overall, GoHam b consists of a small (of the order of 100 AU) and dense (of the order of  $10^7 \, \mathrm{cm}^{-3}$ ) structure of molecular gas and dust, with a mass of  $0.8-11.4 \, \mathrm{M}_{Jup}$  (for a dust-to-gas mass ratio of 0.01). These results are fully consistent with those of Bujarrabal et al. (2009), which in addition have shown that the position of GoHam b corresponds to a modification of the Keplerian velocity field. Altogether, this evidence indicates that GoHam b is a promising candidate of protoplanet formed by gravitational instability. Further studies, in particular at higher angular resolution and with other tracers using ALMA coupled to detailed 3D radiative transfer modeling, are needed to confirm this hypothesis and to rule out other possibilities (such as the presence of an arc of gas and dust).

Acknowledgements. This work was supported by the CNRS program "Physique et Chimie du Milieu Interstellaire" (PCMI)

# References

Acke, B. & van den Ancker, M. E. 2004, A&A, 426, 151 Andrews, S. M., Wilner, D. J., Hughes, A. M., Qi, C., & Dullemond, C. P. 2009. ApJ, 700, 1502 Avenhaus, H., Quanz, S. P., Schmid, H. M., et al. 2014, ApJ, 781, 87 Bailey, V., Meshkat, T., Reiter, M., et al. 2014, ApJ, 780, L4 Berné, O., Joblin, C., Fuente, A., & Ménard, F. 2009, A&A, 495, 827 Boccaletti, A., Pantin, E., Lagrange, A.-M., et al. 2013, A&A, 560, A20 Boley, A. C., Hayfield, T., Mayer, L., & Durisen, R. H. 2010, Icarus, 207, 509 Boss, A. P. 1997, Science, 276, 1836 Bruderer, S., van der Marel, N., van Dishoeck, E. F., & van Kempen, T. A. 2014, A&A, 562, A26 Bujarrabal, V., Young, K., & Castro-Carrizo, A. 2009, A&A, 500, 1077 Bujarrabal, V., Young, К., & Fong, D. 2008, A&A, 483, 839 Casassus, S., Perez M., S., Jordán, A., et al. 2012, ApJ, 754, L31 Casassus, S., van der Plas, G., M, S. P., et al. 2013, Nature, 493, 191 Currie, T., Muto, T., Kudo, T., et al. 2014, ApJ, 796, L30 D'Alessio, P., Calvet, N., & Hartmann, L. 2001, ApJ, 553, 321 De Beck, E., Decin, L., de Koter, A., et al. 2010, A&A, 523, A18 Dutrey, A., di Folco, E., Guilloteau, S., et al. 2014, Nature, 514, 600 Grady, C. A., Muto, T., Hashimoto, J., et al. 2013, ApJ, 762, 48 Habart, E., Natta, A., & Krügel, E. 2004, A&A, 427, 179 Joblin, C., Pilleri, P., Montillaud, J., et al. 2010, A&A, 521, L25 Lagrange, A.-M., Bonnefoy, M., Chauvin, G., et al. 2010, Science, 329, 57 Marois, C., Zuckerman, B., Konopacky, Q. M., Macintosh, B., & Barman, T. 2010, Nature, 468, 1080 Mecus, G., Waters, L. B. F. M., Bouwman, J., et al. 2001, A&A, 365, 476 Muto, T., Grady, C. A., Hashimoto, J., et al. 2012, ApJ, 748, L22 Perrin, M. D., Duchêne, G., Kalas, P., & Graham, J. R. 2006, ApJ, 645, 1272 Pilleri, P., Montillaud, J., Berné, O., & Joblin, C. 2012, A&A, 542, A69 Quanz, S. P., Amara, A., Meyer, M. R., et al. 2014, ArXiv e-prints [arXiv:1412.5173] Quanz, S. P., Amara, A., Meyer, M. R., et al. 2013, ApJ, 766, L1 Quanz, S. P., Beuther, H., Steinacker, J., et al. 2010, ApJ, 717, 693 Rameau, J., Chauvin, G., Lagrange, A.-M., et al. 2012, A&A, 546, A24

Rathborne, J. M., Jackson, J. M., & Simon, R. 2006, ApJ, 641, 389
Ruiz, M. T., Blanco, V., Maza, J., et al. 1987, ApJ, 316, L21
Stapelfeldt, K. R., Watson, A. M., Krist, J. E., et al. 1999, ApJ, 516, L95
Tang, Y.-W., Guilloteau, S., Piétu, V., et al. 2012, A&A, 547, A84
Tielens, A. G. G. M. 2008, ARA&A, 46, 289
Toomre, A. 1964, ApJ, 139, 1217
van der Marel, N., van Dishoeck, E. F., Bruderer, S., et al. 2013, Science, 340, 1199
Weingartner, J. C. & Draine, B. T. 2001, ApJ, 548, 296
Wood, K., Whitney, B. A., Robitaille, T., & Draine, B. T. 2008, ApJ, 688, 1118

# Appendix A: Supplementary Figure

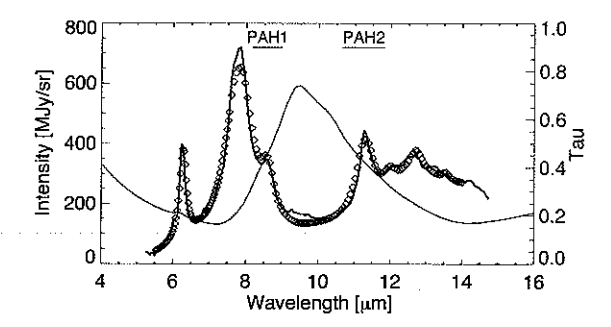


Fig. A.1. Spitzer IRS spectrum of GoHam (continuous black line) and fit (diamonds) using the PAHTAT model. The mid-IR optical depth derived by the model is shown in red. The positions and bandwidths of the VISIR PAH1 and PAH2 filters are indicated. This spectrum includes GoHam a and b, the absorption is dominated by the disk mid-plane.

# Appendix B: Model

#### Appendix B.1: Model description

We model GoHam b as a spherical clump of constant density  $n_b$  and radius  $r_b$ . The presence of this clump results in a localized excess of column density with a profile along the cut as a function of position p (Fig. 3) of parabolic form:

$$N_H(p) = n_b \times 2 \Re\left(\sqrt{r_b^2 - (p_b - p)^2}\right)$$
 (B.1)

where  $p_b$  is the position of GoHam b in the cross cut, i.e. 4.25". The resulting mid-IR optical depth  $\tau_b$  due to GoHam b is then:

$$\tau_b(p) = C_{ext} \times N_H(p), \tag{B.2}$$

where  $C_{ext}$  is the dust cross section per unit of H atom. The mid-IR emission along the cut, corrected from the extinction by Go-Ham b, can then be recovered by:

$$I_{IR}^{0}(p) = I_{IR}(p)/\exp(-\tau_b(p)),$$
 (B.3)

where  $I_{IR}(p)$  is the observed mid-IR emission profile shown in Fig. 3. In addition, we compute the emission in the <sup>13</sup>CO(2-1) line as a function of p:

$$I_{CO}(p) = T_{CO}^{peak}(p)\Delta v \Omega_{ff} \otimes K, \tag{B.4}$$

where  $\Delta \nu$  is the width of the line measured to be 1.7 km/s,  $\Omega_{ff}$  is the beam filling factor equal to  $(a \times b)/r_b^2$ , where a and b are the minor and major axis of the beam, i.e. a=1.14'' and b=1.52''. K is a gaussian kernel of width equal to b, which is the angular resolution along the cut shown in Fig. 3 (since the major axis of the beam is almost aligned North-South—see Bujarrabal et al. 2009— as well as our cross cut).  $T_{CO}^{peak}(p)$  is the brightness temperature of the  $^{13}\text{CO}(2-1)$  line which is equal to zero for  $p < p_b - r_b$  and  $p > p_b + r_b$ . For the other values of p, the brightness is equal to (optically thick line):

$$T_{CO}^{peak} = \frac{h\nu}{k} \times \frac{1}{(\exp(h\nu/(kT_{ex})) - 1)},$$
(B.5)

Article number, page 5 of 7

where  $T_{ex}$  is the excitation temperature, which we fix to 16 K, i.e. the temperature of the disk midplane derived by Bujarrabal et al. (2009).  $T_{ex}$  could be larger than this value in the internal parts of the clump, but this is not critical in the estimation of  $r_b$  which is a function of the square root of  $T_{ex}$ . Overall, the parameters of the model are the density of GoHam b  $n_b$ , the radius of GoHam b  $r_b$ , and the dust cross section  $C_{ext}$ . For interstellar dust, the cross section is typically  $C_{ext} = 2.5 \times 10^{-23} \text{ cm}^2$  per H atom at 8.6 and 11.2  $\mu$ m (Weingartner & Draine 2001). In disks, however, this value is expected to decrease significantly due to grain growth, typically by a factor of 10 in the mid-1R (Andrews et al. 2009; D'Alessio et al. 2001). We will therefore consider these two extreme cases and their effects on the parameters derived by the model.

## Appendix B.2: Adjustment of the parameters $n_b$ and $r_b$

First,  $r_b$  is adjusted so as to reproduce the observed emission profile of  $I_{CO}$  as shown in Fig. 3. Once the value of  $r_b$  is adjusted, the following step consists in adjusting the parameter  $n_b$  so as to obtain a symmetric  $I_{IR}^0(p)$  profile which is what is expected in a disk without any clump. The result of this procedure is shown in Fig. 3. From the adjusted values of  $n_b$  and  $r_b$ , we can derive the clump mass:

$$M_b = 4/3 \pi r_b^3 \times n_b \mu m_H, (B.6)$$

where  $\mu$  is the mean molecular weight and  $m_H$  the proton mass. The parameters used in the model and those derived from the fit for the two values of  $C_{ext}$  are summarized in Table B.2.

O. Berné et al.: Very Large Telescope observations of Gomez's Hamburger: Insights into a young protoplanet candidate

Table B.1. Main physical parameters of the GoHam disk. Error bars result from the uncertainty on distance to GoHam.

Parameter		Comment	Ref.	
GoHam a				
d	$250 \pm 50 \text{ pc}$	Distance	(1,2,3)	
$M_*$	$2.5 \pm 0.5 \ M_{\odot}$	Mass of the star1	(1)	
$R_{PAH}$	$750 \pm 150 \text{ AU}$	See Fig. 2	(4)	
$R_{mol}$	$1650 \pm 350 \text{ AU}$	See Fig. 2	(1)	
$H_{PAH}$	$775 \pm 150 \text{ AU}$	See Fig. 2	(4)	
$H_{mol}$	$450 \pm 90 \text{ AU}$	See Fig. 2	(1)	
n	$> 10^6 { m cm}^{-3}$	Midplane density <sup>2</sup>	(1)	
T ·	16 K	Midplane gas temp. <sup>3</sup>	(1)	

<sup>(1)</sup> Bujarrabal et al. 2009 (2) Berné et al. 2009 (3) Wood et al. 2008 (4) This work

Table B.2. Main physical parameters of the GoHam b candidate protoplanet in the model. Error bars result from the uncertainty on adjustment of the model and on distance to GoHam (the latter being dominant). The values in parenthesis correspond to the case when  $C_{ext}$  is a factor of 10 smaller than the ISM value, i.e.  $C_{ext} = 2.5 \times 10^{-24}$  cm<sup>2</sup>/H.

Input parameters				
$C_{ext}$	$2.5 \times 10^{-23}$ ( $2.5 \times 10^{-24}$ )	Mid-IR dust cross section in cm <sup>2</sup> /H		
$p_b$	4.25	Position of GoHam b in cross cut Fig. 3 (")		
Δν	1.7	Width of the <sup>13</sup> CO line in km/s		
$T_{ex}$	16	CO Excitation temperature in K		
Output parameters				
$r_b$	$155 \pm 31$	Clump radius in AU		
$M_b$	$0.95 \pm 0.19  (9.5 \pm 1.9)$	Clump mass in Jupiter mass		
$n_b$	$7.0 \pm 1.4 \times 10^6 \ (7.0 \pm 1.4 \times 10^7)$	Clump density in cm <sup>-3</sup>		

<sup>&</sup>lt;sup>1</sup> From the keplerian velocity field. <sup>2</sup> Lower limit from CO observations

 $<sup>^3</sup>$  Assumed to be uniform with radius.  $^4\mbox{For a dust-to-gas mass ratio of }0.01$